Self-adaptive Interfacial Glue for Low-pressure Sulfide-Based All-Solid-State Lithium Metal Batteries

Dengxu Wu[1-2], Ziqi Zhang[1-5], Lutong Wang[1-5], Lei Zhu[4-6], Hong Li[1-4], Liquan Chen[1-4] & Fan Wu*[1-6]

[1]Key Laboratory for Renewable Energy, Beijing Key Laboratory for New Energy Materials and Devices, Beijing National Laboratory for Condensed Matter Physics, Institute of Physics, Chinese Academy of Sciences, Beijing, 100190, China
[2]University of Chinese Academy of Sciences, Beijing, 100049, China
[3]Yangtze River Delta Physics Research Center, Liyang 213300, Jiangsu, China
[4]Tianmu Lake Institute of Advanced Energy Storage Technologies, Liyang 213300, Jiangsu, China
[5]CASOL Energy Co ltd, liyang 213399, China
[6]Nano Science and Technology Institute, University of Science and Technology of China, Suzhou 215123, China

*Corresponding author: Fan Wu
E-mail: fwu@iphy.ac.cn

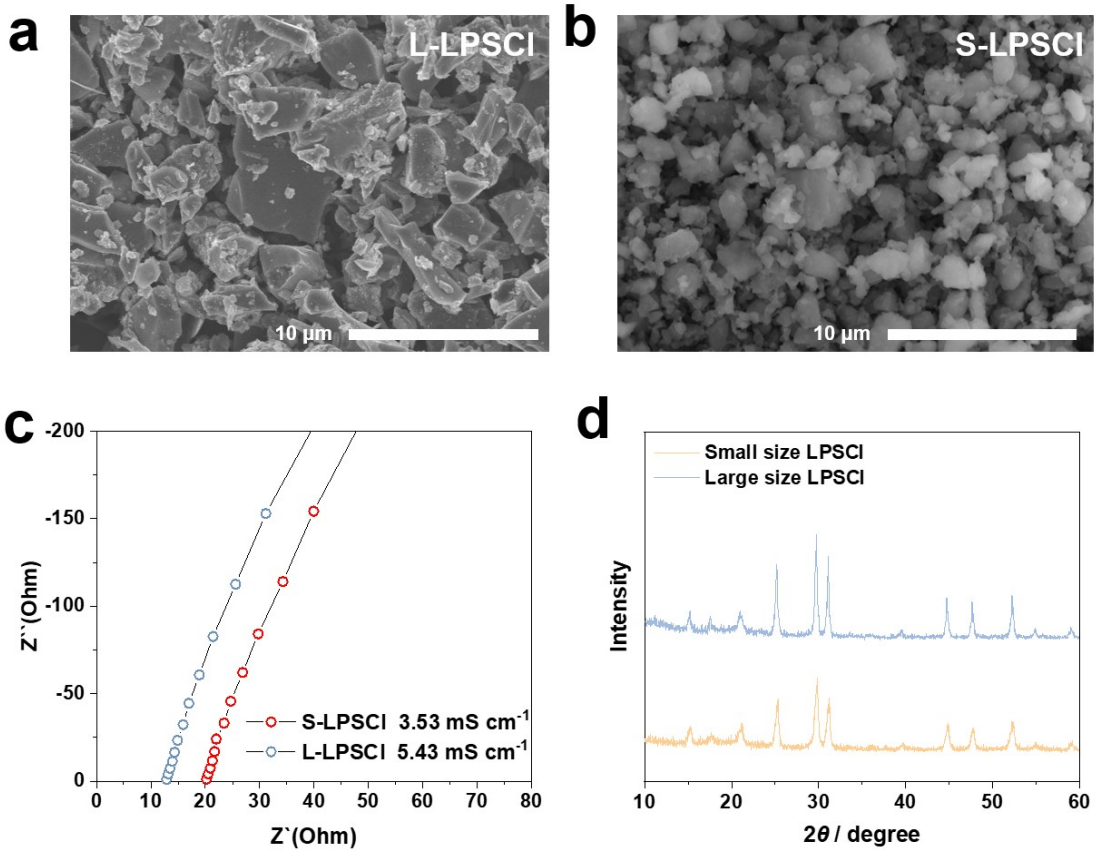

Supplementary Fig. 1 | The SEM images of L-LPSCl (**a**) and S-LPSCl (**b**). The EIS data (**c**) and XRD profiles (**d**) of L-LPSCl and S-LPSCl.

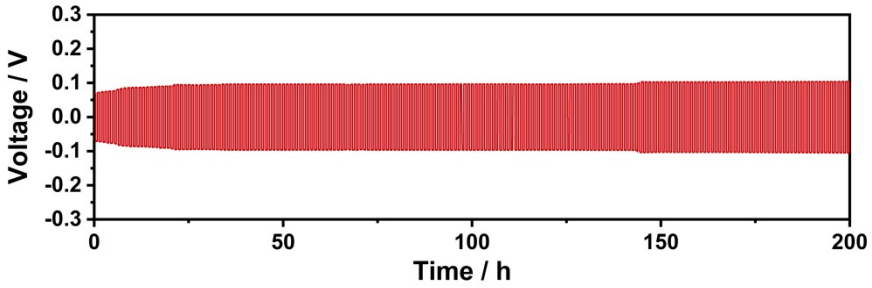

Supplementary Fig. 2 | Voltage curves of symmetric Li | S-LPSCl | Li cell under a high current density of 2 mA cm^{-2}.

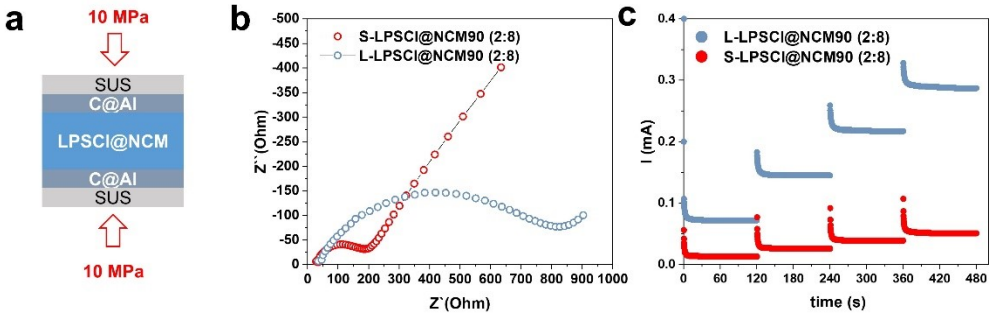

Supplementary Fig. 3 | **a**, The schematic of testing device. **b**, EIS data of L/S-LPSCl@NCM composite. **c,** CA measurement results for L/S-LPSCl@NCM composite at 0.1–0.5.

Supplementary Table 1 | Summary of resistance and calculated electronic conductivity (σ_e) of composite cathode (S-LPSCl@NCM90@x% VGCF, x=0, 1, 2, 3) under 10 MPa pressure.

Sample	**Resistance [Ω]**	σ_e **[S cm^{-1}]**
NCM@0 wt% VGCF	7.87×10^{3}	9.71×10^{-6}
NCM@1 wt% VGCF	1.16×10^{3}	6.89×10^{-5}
NCM@2 wt% VGCF	1.00×10	7.64×10^{-3}
NCM@3 wt% VGCF	1.30	5.88×10^{-2}

Chronoamperometry (CA) was measured in the range from 0.1 V to 0.4 V. Regarding each values, the current is the average of the last 100 points measured data at each voltage. On the other hand, the resistance (R) value was obtained by plotting current values from 0.1 V to 0.4 V and calculating the slope through the slope (1/R) using a linear fit. Finally, electronic conductivity was calculated using the R obtained through linear fit.

Supplementary Table 2 | Summary of electronic conductivity (σ_e) and ionic conductivity (σ_{ion}) of composite cathode (S-LPSCl@NCM90@2% VGCF) under different stack pressure.

Pressure	σ_{ion} **[mS cm^{-1}]**	σ_e **[mS cm^{-1}]**
2 MPa	0.366	7.18
5 MPa	0.370	7.41
10 MPa	0.376	7.66
15 MPa	0.384	8.03
20 MPa	0.396	8.24
25 MPa	0.406	8.40

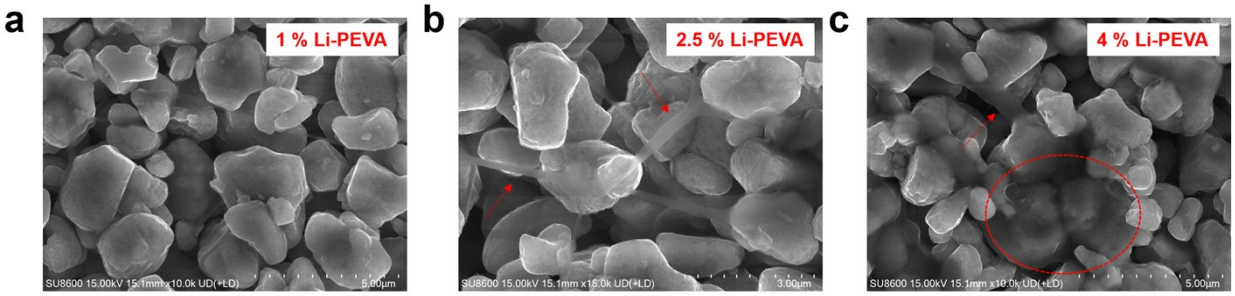

Supplementary Fig. 4 | SEM images of NCM particles with different Li-PEVA content: (a) 1 wt%, (b) 2.5 wt%, (c) 4 wt%.

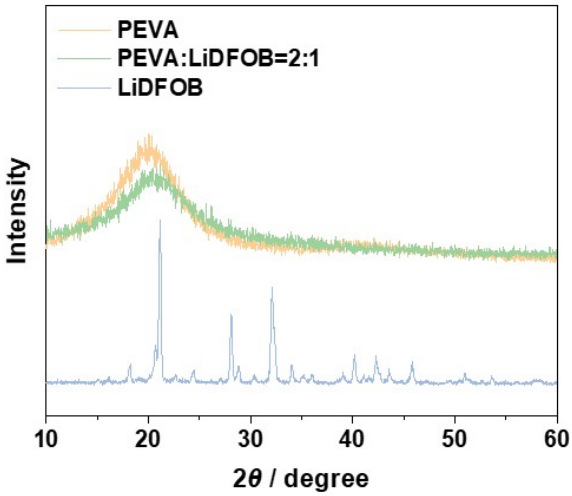

Supplementary Fig. 5 | XRD pattern of PEVA, PEVA-LiDFOB and LiDFOB.

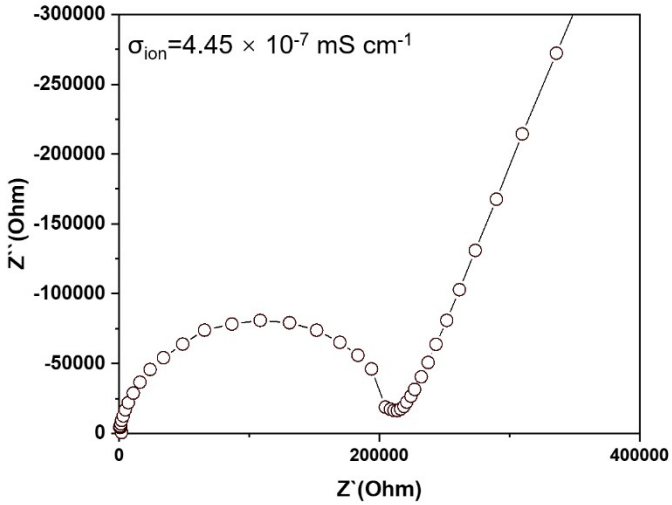

Supplementary Fig. 6 | EIS data for PEVA-LiDFOB (mass ratio: 3:2) composite.

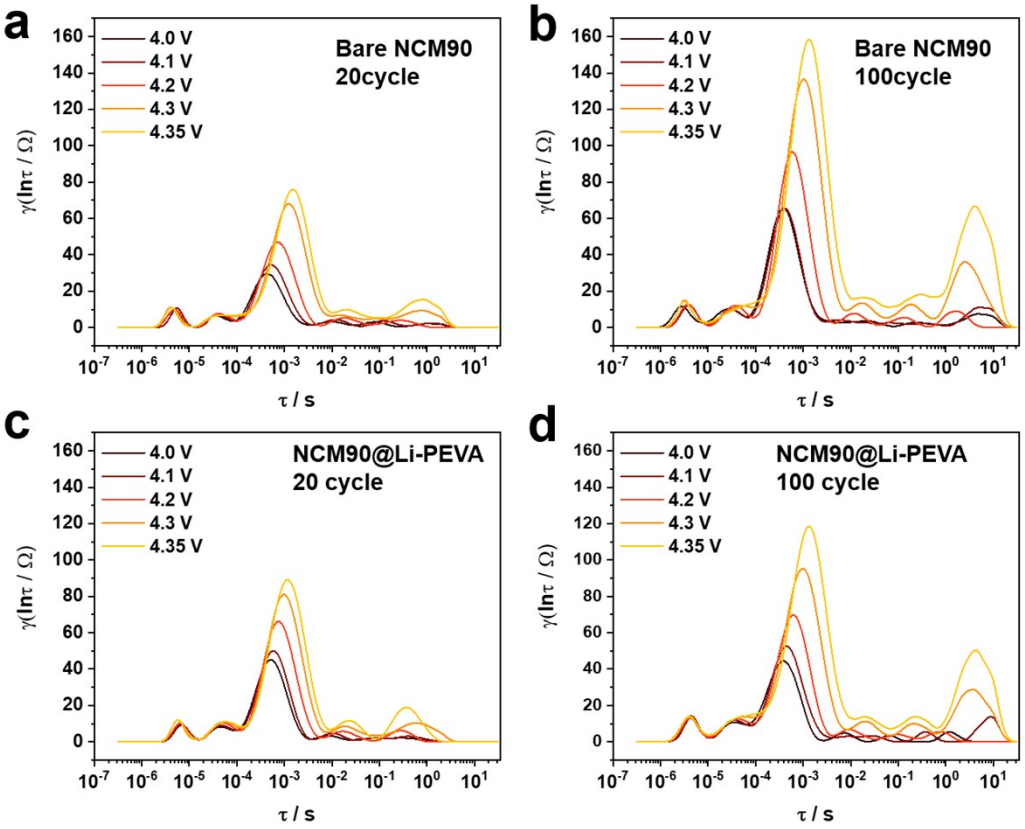

Supplementary Fig. 7 | DRT plot calculated from EIS measurements at different voltages. **a**, bare NCM90 cell after 20 cycles. **b**, bare NCM90 cell after 100 cycles. **c**, NCM90@Li-PEVA cell after 20 cycles. **d**, NCM90@Li-PEVA cell after 100 cycles.

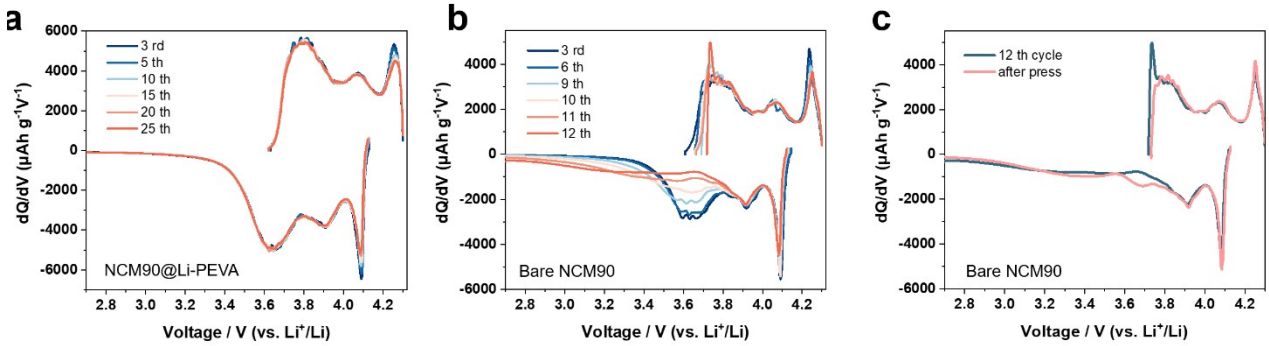

Supplementary Fig. 8 | dQ/dV curves for NCM 90@Li-PEVA and bare NCM90 batteries under 2 mAh cm^{-2} areal capacity and 2 MPa stack pressure.

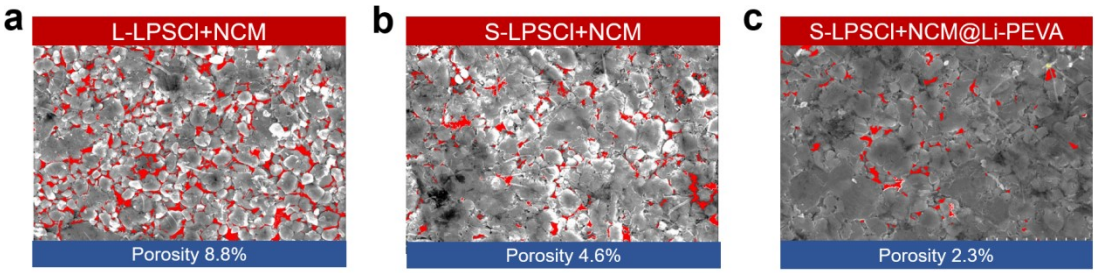

Supplementary Fig. 9 | SEM images of L-LPSCl+NCM cathode (**a**), S-LPSCl+NCM cathode (**b**) and S-LPSCl+NCM@Li-PEVA cathode (**c**) and their porosity analysis through ImageJ software.

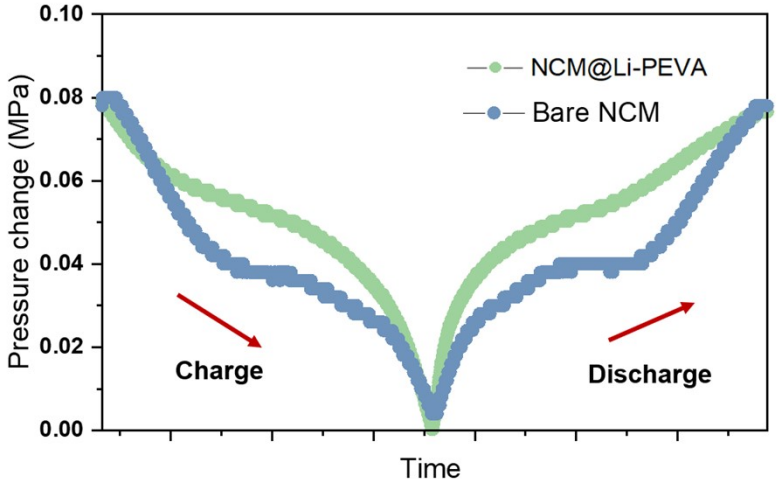

Supplementary Fig. 10 | Pressure changes for bare NCM/LTO and NCM@Li-PEVA/LTO batteries during cycling.

The cathode composite (10 mg) and the electrolyte (80 mg) were laminated following the aforementioned procedure. The anode was prepared using the zero-strain material $Li_4Ti_5O_{12}$ (LTO). A composite of LTO, LPSC, and vapor-grown carbon fiber (VGCF) in a mass ratio of 35:60:5 was prepared by hand grinding. This anode composite (30 mg) was then uniformly spread on the opposite side of the LPSC pellet and pressed at 360 MPa. The assembled cell was tested under a constant stack pressure of 10 MPa. The pressure variation shown in the figure corresponds to data from the tenth cycle.

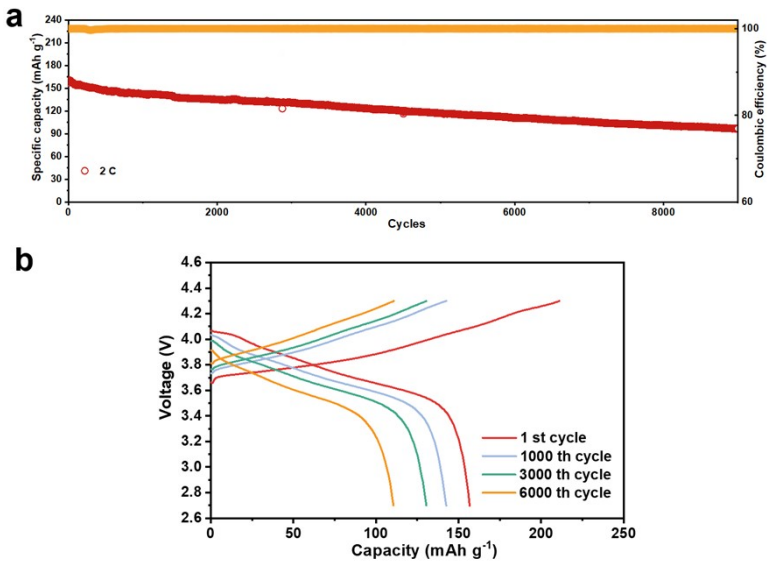

Supplementary Fig. 11. (a) Long-term cycling performance of ASSLBs with NCM90@Li-PEVA composite cathodes under 2C at room temperature (RT) and 10 MPa stack pressure. (b) The charge/discharge curves of different cycles.

Supplementary Table 3 | The summary of electrochemical performances of reported sulfide-based all-solid-state batteries with NCM cathode under low stack pressure and room temperature.

Number	Battery Configuration	Number of cycles	Rate	Capacity (mAh g^{-1})	Capacity retention rate	Stack pressure	Reference
1	DPF-NCA/LPSC/Li	2000	0.2 C	150	65%	2.5 MPa	[1]
2	NCM/LPSCl/Ag-coated Si	200	0.2 C	146	59%	15 MPa	[2]
3	NCM/LPSCl/MgSiGr	75	0.2C	170	83.7%	20 MPa	[3]
4	NCM/LPSX/LTO	150	0.2 C	154	72.8%	2 MPa	[4]
5	NCM/LPSnS /LiIn	150	0.2 C	161	92.6%	3 MPa	[5]
6	NCM/LPSCl/W/Mg	200	3 C	130	86.7%	15 MPa	[6]
7	NMC/LPSCl/Mg/W-Cu	150	0.33 C	140	75%	14 MPa	[7]
8	NCM/LPSCl/LPSCl@Li	800	2C	80	76.3%	Coin cell	[8]
9	AZ@NCM/LPSCl/LiIn	50	0.2 C	169.5	90.8%	2 MPa	[9]
10	NMC/LPSCl-$AlCl_3$/Li	2200	0.8 C	110	81%	5 MPa	[10]
This work	NCM@Li-PEVA/LPSCl/Li	1000	1C	176	90.9%	10 MPa	This work
		3000	2C	160	80%	10 MPa	This work

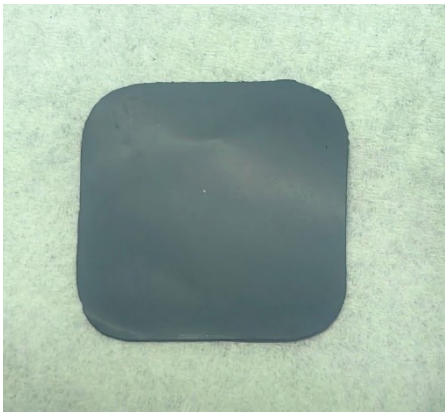

Supplementary Fig. 12 | Composite cathode dry film with 0.2wt% PTFE.

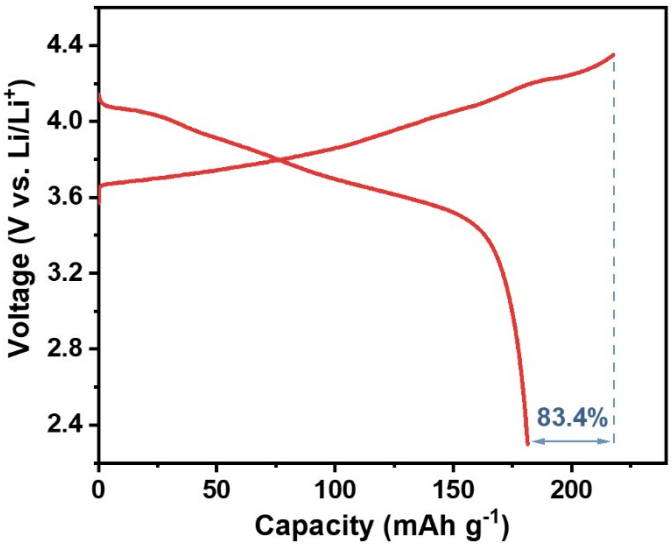

Supplementary Fig. 13 | Initial charge-discharge voltage profiles of the pouch cell at 0.2C when measured at 25°C and 2 MPa.

Supplementary Table 4 | Information for calculating the energy density of pouch-type ASSLB.

Cell component	Materials	Mass loading (mg cm^{-2})
Cathode	NCM90(80 wt.%)	11.2
SE	LPSCl/PTFE (50um thick)	8.3
Anode	Li-In	14.3
Discharge capacity		18 mAh
Positive electrode area		3×3 cm^{-2}
SE membrane area Negative electrode area		3.2×3.2 cm^{-2}
Average discharge voltage		3.11V
Energy density		170.2 Wh kg^{-1}

Reference

1. Zhang, W. *et al.* Revitalizing interphase in all-solid-state Li metal batteries by electrophile reduction. *Nat. Mater.* **24**, 414–423 (2025).
2. Jun, S. *et al.* Interlayer Engineering and Prelithiation: Empowering Si Anodes for Low-Pressure-Operating All-Solid-State Batteries. *Small* **20**, 2309437 (2024).
3. Oh, J. *et al.* All-Solid-State Batteries with Extremely Low N/P Ratio Operating at Low Stack Pressure. *Advanced Energy Materials* 2404817 (2024) doi:10.1002/aenm.202404817.
4. Kwon, T. Y. *et al.* Three-Dimensional Networking Binders Prepared in situ during Wet-Slurry Process for All-Solid-State Batteries Operating under Low External Pressure. *Energy Storage Materials* **49**, 219–226 (2022).
5. Woo, J. *et al.* Liquid-Phase Synthesis of Highly Deformable and Air-Stable Sn-Substituted Li_3PS_4 for All-Solid-State Batteries Fabricated and Operated under Low Pressures. *Advanced Energy Materials* **13**, 2203292 (2023).
6. Oh, J. *et al.* Lithio-amphiphilic nanobilayer for high energy density anode-less all-solid-state batteries operating under low stack pressure. *Energy Environ. Sci.* **17**, 7932–7943 (2024).
7. Wang, Y. *et al.* Control of Two Solid Electrolyte Interphases at the Negative Electrode of an Anode-Free All Solid-State Battery based on Argyrodite Electrolyte. *Advanced Materials* 2410948 (2025) doi:10.1002/adma.202410948.
8. Li, J. *et al.* Self-Limiting Reaction of Solid Electrolyte Empowering Ultralong Lifespan All-Solid-State Lithium Metal Batteries with Li6PS5Cl-Based Electrolyte Membrane. *Advanced Functional Materials* 2504546 (2025) doi:10.1002/adfm.202504546.
9. Ge, Z. *et al.* Constructing dendrite suppressing mixed sulfide solid electrolyte for high-rate lithium metal batteries. *Chemical Engineering Journal* **467**, 143409 (2023).
10. Ren, P. *et al.* Scalable Interfacial Engineering with Lithiophilic-Lithiophobic Layers for High-Performance All-Solid-State Li-Metal Batteries. *Adv Funct Materials* 2501573 (2025) doi:10.1002/adfm.202501573.